EUROPEAN ORGANIZATION FOR NUCLEAR RESEARCH (CERN)

CERN–PPE/95–125
18 August 1995

Measurement of the B_s^0 lifetime and production rate with D_s^- ℓ^+ combinations in Z decays

The ALEPH Collaboration

Abstract

The lifetime of the B_s^0 meson is measured in approximately 3 million hadronic Z decays accumulated using the ALEPH detector at LEP from 1991 to 1994. Seven different D_s^- decay modes were reconstructed and combined with an opposite sign lepton as evidence of semileptonic B_s^0 decays. Two hundred and eight $D_s^-\ell^+$ candidates satisfy selection criteria designed to ensure precise proper time reconstruction and yield a measured B_s^0 lifetime of $\tau(B_s^0) = 1.59\ ^{+0.17}_{-0.15}$ (stat) $\pm$ 0.03 (syst) ps . Using a larger, less constrained sample of events, the product branching ratio is measured to be $Br(\overline{b} \to B_s^0) \cdot Br(B_s^0 \to D_s^-\ell^+\nu X) = 0.82\ \pm 0.09$ (stat) $^{+0.13}_{-0.14}$ (syst) %.

(Submitted to Physics Letters B.)

The ALEPH Collaboration

D. Buskulic, D. Casper, I. De Bonis, D. Decamp, P. Ghez, C. Goy, J.-P. Lees, A. Lucotte, M.-N. Minard, P. Odier, B. Pietrzyk

Laboratoire de Physique des Particules (LAPP), IN^{2}P^3-CNRS, 74019 Annecy-le-Vieux Cedex, France

F. Ariztizabal, M. Chmeissani, J.M. Crespo, I. Efthymiopoulos, E. Fernandez, M. Fernandez-Bosman, V. Gaitan, Ll. Garrido,[15] M. Martinez, S. Orteu, A. Pacheco, C. Padilla, F. Palla, A. Pascual, J.A. Perlas, F. Sanchez, F. Teubert

Institut de Fisica d'Altes Energies, Universitat Autonoma de Barcelona, 08193 Bellaterra (Barcelona), Spain[7]

A. Colaleo, D. Creanza, M. de Palma, A. Farilla, G. Gelao, M. Girone, G. Iaselli, G. Maggi,[3] M. Maggi, N. Marinelli, S. Natali, S. Nuzzo, A. Ranieri, G. Raso, F. Romano, F. Ruggieri, G. Selvaggi, L. Silvestris, P. Tempesta, G. Zito

Dipartimento di Fisica, INFN Sezione di Bari, 70126 Bari, Italy

X. Huang, J. Lin, Q. Ouyang, T. Wang, Y. Xie, R. Xu, S. Xue, J. Zhang, L. Zhang, W. Zhao

Institute of High-Energy Physics, Academia Sinica, Beijing, The People's Republic of China[8]

G. Bonvicini, M. Cattaneo, P. Comas, P. Coyle, H. Drevermann, A. Engelhardt, R.W. Forty, M. Frank, R. Hagelberg, J. Harvey, R. Jacobsen,[24] P. Janot, B. Jost, J. Knobloch, I. Lehraus, C. Markou,[23] E.B. Martin, P. Mato, H. Meinhard, A. Minten, R. Miquel, T. Oest, P. Palazzi, J.R. Pater,[27] J.-F. Pusztaszeri, F. Ranjard, P. Rensing, L. Rolandi, D. Schlatter, M. Schmelling, O. Schneider, W. Tejessy, I.R. Tomalin, A. Venturi, H. Wachsmuth, W. Wiedenmann, T. Wildish, W. Witzeling, J. Wotschack

European Laboratory for Particle Physics (CERN), 1211 Geneva 23, Switzerland

Z. Ajaltouni, M. Bardadin-Otwinowska,[2] A. Barres, C. Boyer, A. Falvard, P. Gay, C. Guicheney, P. Henrard, J. Jousset, B. Michel, S. Monteil, J-C. Montret, D. Pallin, P. Perret, F. Podlyski, J. Proriol, J.-M. Rossignol, F. Saadi

Laboratoire de Physique Corpusculaire, Université Blaise Pascal, IN^{2}P^3-CNRS, Clermont-Ferrand, 63177 Aubière, France

T. Fearnley, J.B. Hansen, J.D. Hansen, J.R. Hansen, P.H. Hansen, B.S. Nilsson

Niels Bohr Institute, 2100 Copenhagen, Denmark[9]

A. Kyriakis, E. Simopoulou, I. Siotis, A. Vayaki, K. Zachariadou

Nuclear Research Center Demokritos (NRCD), Athens, Greece

A. Blondel,[21] G. Bonneaud, J.C. Brient, P. Bourdon, L. Passalacqua, A. Rougé, M. Rumpf, R. Tanaka, A. Valassi,[31] M. Verderi, H. Videau

Laboratoire de Physique Nucléaire et des Hautes Energies, Ecole Polytechnique, IN^{2}P^3-CNRS, 91128 Palaiseau Cedex, France

D.J. Candlin, M.I. Parsons

Department of Physics, University of Edinburgh, Edinburgh EH9 3JZ, United Kingdom[10]

E. Focardi, G. Parrini

Dipartimento di Fisica, Università di Firenze, INFN Sezione di Firenze, 50125 Firenze, Italy

M. Corden, M. Delfino,[12] C. Georgiopoulos, D.E. Jaffe

Supercomputer Computations Research Institute, Florida State University, Tallahassee, FL 32306-4052, USA [13,14]

A. Antonelli, G. Bencivenni, G. Bologna,[4] F. Bossi, P. Campana, G. Capon, V. Chiarella, G. Felici, P. Laurelli, G. Mannocchi,[5] F. Murtas, G.P. Murtas, M. Pepe-Altarelli

Laboratori Nazionali dell'INFN (LNF-INFN), 00044 Frascati, Italy

S.J. Dorris, A.W. Halley, I. ten Have,[6] I.G. Knowles, J.G. Lynch, W.T. Morton, V. O'Shea, C. Raine, P. Reeves, J.M. Scarr, K. Smith, M.G. Smith, A.S. Thompson, F. Thomson, S. Thorn, R.M. Turnbull

Department of Physics and Astronomy, University of Glasgow, Glasgow G12 8QQ,United Kingdom[10]

U. Becker, O. Braun, C. Geweniger, G. Graefe, P. Hanke, V. Hepp, E.E. Kluge, A. Putzer, B. Rensch, M. Schmidt, J. Sommer, H. Stenzel, K. Tittel, S. Werner, M. Wunsch

Institut für Hochenergiephysik, Universität Heidelberg, 69120 Heidelberg, Fed. Rep. of Germany[16]

R. Beuselinck, D.M. Binnie, W. Cameron, D.J. Colling, P.J. Dornan, N. Konstantinidis, L. Moneta, A. Moutoussi, J. Nash, G. San Martin, J.K. Sedgbeer, A.M. Stacey

Department of Physics, Imperial College, London SW7 2BZ, United Kingdom[10]

G. Dissertori, P. Girtler, E. Kneringer, D. Kuhn, G. Rudolph

Institut für Experimentalphysik, Universität Innsbruck, 6020 Innsbruck, Austria[18]

C.K. Bowdery, T.J. Brodbeck, P. Colrain, G. Crawford, A.J. Finch, F. Foster, G. Hughes, T. Sloan, E.P. Whelan, M.I. Williams

Department of Physics, University of Lancaster, Lancaster LA1 4YB, United Kingdom[10]

A. Galla, A.M. Greene, K. Kleinknecht, G. Quast, J. Raab, B. Renk, H.-G. Sander, R. Wanke, P. van Gemmeren C. Zeitnitz

Institut für Physik, Universität Mainz, 55099 Mainz, Fed. Rep. of Germany[16]

J.J. Aubert, A.M. Bencheikh, C. Benchouk, A. Bonissent,[21] G. Bujosa, D. Calvet, J. Carr, C. Diaconu, F. Etienne, M. Thulasidas, D. Nicod, P. Payre, D. Rousseau, M. Talby

Centre de Physique des Particules, Faculté des Sciences de Luminy, IN^{2}P^3-CNRS, 13288 Marseille, France

I. Abt, R. Assmann, C. Bauer, W. Blum, D. Brown,[24] H. Dietl, F. Dydak,[21] G. Ganis, C. Gotzhein, K. Jakobs, H. Kroha, G. Lütjens, G. Lutz, W. Männer, H.-G. Moser, R. Richter, A. Rosado-Schlosser, S. Schael, R. Settles, H. Seywerd, U. Stierlin,[2] R. St. Denis, G. Wolf

Max-Planck-Institut für Physik, Werner-Heisenberg-Institut, 80805 München, Fed. Rep. of Germany[16]

R. Alemany, J. Boucrot, O. Callot, A. Cordier, F. Courault, M. Davier, L. Duflot, J.-F. Grivaz, Ph. Heusse, M. Jacquet, D.W. Kim,[19] F. Le Diberder, J. Lefrançois, A.-M. Lutz, G. Musolino, I. Nikolic, H.J. Park, I.C. Park, M.-H. Schune, S. Simion, J.-J. Veillet, I. Videau

Laboratoire de l'Accélérateur Linéaire, Université de Paris-Sud, IN^{2}P^3-CNRS, 91405 Orsay Cedex, France

D. Abbaneo, P. Azzurri, G. Bagliesi, G. Batignani, S. Bettarini, C. Bozzi, G. Calderini, M. Carpinelli, M.A. Ciocci, V. Ciulli, R. Dell'Orso, R. Fantechi, I. Ferrante, L. Foà,[1] F. Forti, A. Giassi, M.A. Giorgi, A. Gregorio, F. Ligabue, A. Lusiani, P.S. Marrocchesi, A. Messineo, G. Rizzo, G. Sanguinetti, A. Sciabà, P. Spagnolo, J. Steinberger, R. Tenchini, G. Tonelli,[26] G. Triggiani, C. Vannini, P.G. Verdini, J. Walsh

Dipartimento di Fisica dell'Università, INFN Sezione di Pisa, e Scuola Normale Superiore, 56010 Pisa, Italy

A.P. Betteridge, G.A. Blair, L.M. Bryant, F. Cerutti, Y. Gao, M.G. Green, D.L. Johnson, T. Medcalf, Ll.M. Mir, P. Perrodo, J.A. Strong

Department of Physics, Royal Holloway & Bedford New College, University of London, Surrey TW20 OEX, United Kingdom[10]

V. Bertin, D.R. Botterill, R.W. Clifft, T.R. Edgecock, S. Haywood, M. Edwards, P. Maley, P.R. Norton, J.C. Thompson

Particle Physics Dept., Rutherford Appleton Laboratory, Chilton, Didcot, Oxon OX11 OQX, United Kingdom[10]

B. Bloch-Devaux, P. Colas, H. Duarte, S. Emery, W. Kozanecki, E. Lançon, M.C. Lemaire, E. Locci, B. Marx, P. Perez, J. Rander, J.-F. Renardy, A. Rosowsky, A. Roussarie, J.-P. Schuller, J. Schwindling, D. Si Mohand, A. Trabelsi, B. Vallage

CEA, DAPNIA/Service de Physique des Particules, CE-Saclay, 91191 Gif-sur-Yvette Cedex, France[17]

R.P. Johnson, H.Y. Kim, A.M. Litke, M.A. McNeil, G. Taylor

Institute for Particle Physics, University of California at Santa Cruz, Santa Cruz, CA 95064, USA[22]

A. Beddall, C.N. Booth, R. Boswell, S. Cartwright, F. Combley, I. Dawson, A. Koksal, M. Letho, W.M. Newton, C. Rankin, L.F. Thompson

Department of Physics, University of Sheffield, Sheffield S3 7RH, United Kingdom[10]

A. Böhrer, S. Brandt, G. Cowan, E. Feigl, C. Grupen, G. Lutters, J. Minguet-Rodriguez, F. Rivera,[25] P. Saraiva, L. Smolik, F. Stephan,

Fachbereich Physik, Universität Siegen, 57068 Siegen, Fed. Rep. of Germany[16]

M. Apollonio, L. Bosisio, R. Della Marina, G. Giannini, B. Gobbo, F. Ragusa[20]

Dipartimento di Fisica, Università di Trieste e INFN Sezione di Trieste, 34127 Trieste, Italy

J. Rothberg, S. Wasserbaech

Experimental Elementary Particle Physics, University of Washington, WA 98195 Seattle, U.S.A.

S.R. Armstrong, L. Bellantoni,[30] P. Elmer, Z. Feng, D.P.S. Ferguson, Y.S. Gao, S. González, J. Grahl, J.L. Harton,[28] O.J. Hayes, H. Hu, P.A. McNamara III, J.M. Nachtman, W. Orejudos, Y.B. Pan, Y. Saadi, M. Schmitt, I.J. Scott, V. Sharma,[29] J.D. Turk, A.M. Walsh, Sau Lan Wu, X. Wu, J.M. Yamartino, M. Zheng, G. Zobernig

Department of Physics, University of Wisconsin, Madison, WI 53706, USA[11]

---

[1] Now at CERN, 1211 Geneva 23, Switzerland.
[2] Deceased.
[3] Now at Dipartimento di Fisica, Università di Lecce, 73100 Lecce, Italy.
[4] Also Istituto di Fisica Generale, Università di Torino, Torino, Italy.
[5] Also Istituto di Cosmo-Geofisica del C.N.R., Torino, Italy.
[6] Now at TSM Business School, Enschede, The Netherlands.
[7] Supported by CICYT, Spain.
[8] Supported by the National Science Foundation of China.
[9] Supported by the Danish Natural Science Research Council.
[10] Supported by the UK Particle Physics and Astronomy Research Council.
[11] Supported by the US Department of Energy, grant DE-FG0295-ER40896.
[12] On leave from Universitat Autonoma de Barcelona, Barcelona, Spain.
[13] Supported by the US Department of Energy, contract DE-FG05-92ER40742.
[14] Supported by the US Department of Energy, contract DE-FC05-85ER250000.
[15] Permanent address: Universitat de Barcelona, 08208 Barcelona, Spain.
[16] Supported by the Bundesministerium für Forschung und Technologie, Fed. Rep. of Germany.
[17] Supported by the Direction des Sciences de la Matière, C.E.A.
[18] Supported by Fonds zur Förderung der wissenschaftlichen Forschung, Austria.
[19] Permanent address: Kangnung National University, Kangnung, Korea.
[20] Now at Dipartimento di Fisica, Università di Milano, Milano, Italy.
[21] Also at CERN, 1211 Geneva 23, Switzerland.
[22] Supported by the US Department of Energy, grant DE-FG03-92ER40689.
[23] Now at University of Athens, 157-71 Athens, Greece.
[24] Now at Lawrence Berkeley Laboratory, Berkeley, CA 94720, USA.
[25] Partially supported by Colciencias, Colombia.
[26] Also at Istituto di Matematica e Fisica, Università di Sassari, Sassari, Italy.
[27] Now at Schuster Laboratory, University of Manchester, Manchester M13 9PL, UK.
[28] Now at Colorado State University, Fort Collins, CO 80523, USA.
[29] Now at University of California at San Diego, La Jolla, CA 92093, USA.
[30] Now at Fermi National Accelerator Laboratory, Batavia, IL 60510, USA.
[31] Supported by the Commission of the European Communities, contract ERBCHBICT941234.

1 Introduction

Measurements of the individual B meson lifetimes provide a well-defined test of the theory of b hadron decays. The lifetimes of the B_d^0 and B_s^0 are expected to be equal to within a few percent and the B^- lifetime is expected to be approximately 5% greater than the neutral B meson[1].

This letter presents the lifetime of the B_s^0 meson measured via reconstructed semileptonic decays, $B_s^0 \to D_s^- \ell^+ \nu X$ [1]. The current measurement improves upon the previous ALEPH result[2] with more than four times the number of observed $D_s^- \ell^+$ combinations by increasing the number of reconstructed D_s^- decay channels from two to seven and making use of approximately 3 million hadronic Z decays recorded from 1991 to 1994. The increased $D_s^- \ell^+$ yield is also used to improve ALEPH's previous measurement[3] of the product branching ratio, $\mathrm{Br}(\bar{b} \to B_s^0) \cdot \mathrm{Br}(B_s^0 \to D_s^- \ell^+ \nu X)$, which is essential to B_s^0 -$\overline{B_s^0}$ oscillation measurements[4, 5, 6], and for determining the various b hadron fractions[7]. The following sections describe the ALEPH detector, the D_s^- and B_s^0 candidate selection, the proper time reconstruction, the lifetime fit and the extraction of the product branching ratio.

2 The ALEPH detector

The ALEPH detector and its performances are described in detail elsewhere[8, 9] and only a brief overview of the apparatus is given here. A high resolution vertex detector (VDET) consisting of two layers of double-sided silicon microstrip detectors surrounds the beam pipe. The inner layer is 6.5 cm from the beam axis and covers 85% of the solid angle and the outer layer is at an average radius of 11.3 cm and covers 69%. The spatial resolution for the $r\phi$ and z projections (transverse to and along the beam axis respectively) is 12 μm at normal incidence. The vertex detector is surrounded by a drift chamber (ITC) with eight coaxial wire layers with an outer radius of 26 cm and by a time projection chamber (TPC) that measures up to 21 three–dimensional points per track at radii between 30 cm and 180 cm. These detectors are immersed in an axial magnetic field of 1.5 T and together measure the momentum of charged particles with a resolution $\sigma(p)/p = 6 \times 10^{-4} p_{\mathrm{T}} \oplus 0.005$ (p in GeV/c). The resolution of the three–dimensional impact parameter in the transverse and longitudinal view for tracks having information from all tracking detectors and two VDET hits can be parameterized as $\sigma = 25\mu\mathrm{m} + 95\mu\mathrm{m}/p$ (p in GeV/c). The TPC also provides up to 338 measurements of the specific ionization of a charged track ($\frac{\mathrm{d}E}{\mathrm{d}x}$). The TPC is surrounded by an electromagnetic calorimeter of lead/proportional–chamber construction segmented into $0.9^\circ \times 0.9^\circ$ projective towers and read out in three sections in depth, with energy resolution $\sigma(E)/E = 0.18/\sqrt{E} + 0.009$ (E in GeV). The iron return yoke of the magnet is instrumented with streamer tubes to form a hadron calorimeter, with a thickness of over 7 interaction lengths and is surrounded by two additional double-layers of streamer tubes to aid in muon identification. An algorithm combines all these measurements to provide a determination of the energy flow[9] with a precision on the measurable total energy of $\sigma(E) = 0.6\sqrt{E/\mathrm{GeV}} + 0.6$ GeV.

The selection of hadronic events is based on charged tracks and is described elsewhere[10]. The interaction point is reconstructed on an event-by-event basis using the constraint of the average beam spot position[11]. The resolution is 85 μm for $\mathrm{Z} \to b\bar{b}$ events, projected along the sphericity axis of the event.

[1] In this paper charge conjugate modes are always implied and "lepton" refers to electrons and muons.

3 Sources of $D_s\ell$ correlations

The five sources of $D_s\ell$ correlations considered are

1. $B_s^0 \to D_s^- \ell^+ \nu X$,
2. $\overline{B} \to D_s^{(*)-} D^{(*)} X$ followed by $D^{(*)} \to \ell^+ \nu X$,
3. $B \to D_s^- X_s \ell^+ \nu$,
4. kinematic reflections in the $D_s^- \to K^{*0}K^-$ ($K_s^0 K^-$) channels due to $D^- \to K^{*0}\pi^-$ ($K_s^0\pi^-$), and
5. combinatorial background.

These different sources of signal and background have been extensively discussed previously [2, 3, 12] and will simply be reviewed here. Only two decays, $B_s^0 \to D_s^{*-}\ell^+\nu$ and $B_s^0 \to D_s^-\ell^+\nu$, are considered to contribute to $B_s^0 \to D_s^-\ell^+\nu X$ as the higher order $\overline{c}s$ resonances decay to $D^{(*)}K$ final states while the $D_s^{*-} \to D_s^-\gamma$ decay dominates[13]. The kinematics of the $\overline{B} \to D_s^{(*)-}D^{(*)}X$ background are simulated by $\overline{B}_d^0 \to D_s^{(*)-}D^{(*)+}(\pi)$ decays but the contributions from B^- , B_s^0 and b baryon decays are included in the rate estimate. The branching ratio of the as-yet unobserved $B \to D_s^- X_s \ell^+\nu$ process is estimated to be less than 0.36% at 90 % C.L. The assumptions and rates used to derive these estimates are discussed in section 8. The reflection background is due to misinterpretation of a charged pion as a charged kaon and is discussed in section 4.1.

4 The $B_s^0 \to D_s^-\ell^+\nu X$ candidate selection

Candidates for $B_s^0 \to D_s^-\ell^+\nu X$ are selected from hadronic Z decays where a D_s^- and a lepton are found in the same hemisphere as defined by the thrust axis. The lepton identification in ALEPH is described in detail in reference[14]. In this paper the requirement that the $\frac{dE}{dx}$ information be available for electron candidates is dropped.

The D_s^- is reconstructed in five hadronic decay modes, $\phi\pi^-$, $K^{*0}K^-$, $\phi\pi^+\pi^-\pi^-$, $K^{*0}K^{*-}$ and $K_s^0K^-$, and two semileptonic decay modes, $\phi e^-\nu$ and $\phi\mu^-\nu$. The selection criteria for the first two modes are similar to those used in the previous B_s^0 lifetime measurement[2]. The next two modes suffer from larger combinatorial background and require more involved selection criteria. The final hadronic mode, $D_s^- \to K_s^0K^-$, is contaminated by the kinematic reflections from $D^- \to K_s^0\pi^-$ requiring more stringent cuts be applied to the charged kaon candidate. The following sections describe the details of the D_s^- selection.

4.1 Kinematic criteria for hadronic D_s^- decays

Each D_s^- candidate must carry at least 15 % of the beam energy. For all the channels the momentum of the charged kaon candidate must be at least 1.5 GeV/c to ensure good kaon and pion $\frac{dE}{dx}$ identification. The charged kaon candidates specific ionization, when available, should fulfil $\chi_\pi + \chi_K < 1$[2], where χ_H is the difference between the measured and expected ionization for the particle hypothesis H in terms of the expected resolution. Pion candidates, except those from the K_s^0 , should have $|\chi_\pi| < 3$ if the $\frac{dE}{dx}$ information is available, and a momentum greater than 0.5 GeV/c. The ϕ , $K^{*+(0)}$ and K_s^0 are reconstructed in the $\phi \to K^+K^-$, $K^{*+(0)} \to K^{0(-)}\pi^+$ and $K_s^0 \to \pi^+\pi^-$ modes and are required to be within 9, 50 and 12 MeV/c^2 of the nominal ϕ , $K^{*+(0)}$ and K_s^0 masses[13], respectively, according to the resolutions and natural widths. The details of the momentum requirements for each hadronic decay mode are summarized in Table 1.

For the $\phi\pi^-$and $K^{*0}K^-$modes, $|\cos\theta^*| > 0.4$ is required, where θ^* is the center-of-mass decay angle of the ϕ or K^{*0} relative to its flight direction. This cut exploits the fact that the distribution

of θ^* is proportional to $\cos^2\theta^*$ for the decay of the pseudoscalar D_s^- into a vector (ϕ or K^{*0}) and a pseudoscalar. To reduce the larger combinatorial background for $K^{*0}K^-$, $|\cos\lambda^*| < 0.8$ is also required where λ^* is the angle of the K^{*0} in the D_s^- center-of-mass relative to the D_s^- flight direction. For the $\phi\pi^+\pi^-\pi^-$ mode, the momentum of at least one pion is required to exceed 1.5 GeV/c and the D_s^- must carry at least 20% of the beam energy.

The $\frac{dE}{dx}$ information is required to be available for the kaon from the D_s^- in the $K^{*0}K^-$ and $K_s^0K^-$ modes to reduce the kinematic reflection background from $D^- \to K^{*0}\pi^-$ and $D^- \to K_s^0\pi^-$, respectively. In addition the kinematic reflection background to $D_s^- \to K_s^0K^-$ from $D^- \to K_s^0\pi^-$ is rendered negligible by requiring $p_K < 5$ GeV/c or $\chi_K < 0$. The kinematic reflection background to $D_s^- \to K_s^0K^-$ from $\Lambda_c^- \to K_s^0\overline{p}$ is also rendered negligible by requiring the invariant mass to be incompatible with the Λ_c^- when the kaon candidate is given the proton mass.

$\phi\pi^-$	$K^{*0}K^-$	$K_s^0K^-$	$\phi\pi^+\pi^-\pi^-$	$K^{*0}K^{*-}$
$p_\phi > 4.0$	$p_{K^*} > 4.0$	$p_{K_s^0} > 2.0$	$p_\phi > 3.5$	$p_{K_s^0} > 2.0$
$p_\pi > 1.0$	$p_{K^-} > 2.0$			$p_{K^-} > 3.0$
	$p_\pi > 1.0$			

Table 1: The momentum cuts in GeV/c for each hadronic D_s^- decay mode. Additional details are described in the text.

4.2 Kinematic criteria for the semileptonic D_s^- decays

The ϕ is reconstructed as in the $\phi\pi^-$ mode. The momentum of the lepton from the D_s^- must be $p_{\mu(e)} > 3(2)$ GeV/c and satisfy the lepton identification criteria cited earlier[14]. Additional electron candidates are identified as tracks satisfying the standard electron criteria with momenta between 1 and 2 GeV/c where the $\frac{dE}{dx}$ information must be available and inconsistent with the proton hypothesis ($|\chi_p| > 2.0$) to eliminate hadron contamination. At 1 GeV/c the electron and proton ionization is indistinguishable.

To unambiguously assign the two leptons (one from the B_s^0, the other from the D_s^-), $M(\phi, \ell_{D_s^-})$ ($M(\phi, \ell_{B_s^0})$) must be at least 15 MeV/c^2 less (more) than the nominal D_s^- mass. If the two leptons are of the same flavour, their invariant mass must be inconsistent[2] with the J/ψ and ψ'; in addition, the mass of electron–positron pairs must be greater than 100 MeV to exclude photon conversions. The $\overline{B} \to D_s^{(*)-}D^{(*)}X$ background is further reduced by requiring the missing energy in the hemisphere, estimated using an energy flow technique[9], to be greater than 10 GeV or the momentum of the lepton from the B_s^0 decay to be greater that 5 GeV/c.

4.3 B_s^0 selection

The tracks forming D_s^- candidates are required to form a vertex in three dimensions and at least two of the charged D_s^- decay products must have at least one $r\phi$ and z VDET hit and at least one ITC hit. For the $D_s^- \to K_s^0K^-$ mode, only the charged kaon track should fulfil this requirement. The D_s^- vertex probability must be greater than 0.01% and the calculated uncertainty on the D_s^- decay length must be less than 1.0 mm.

These D_s^- candidates are in turn used to form a three-dimensional vertex with a candidate lepton with a momentum of at least 3 GeV/c and three-dimensional VDET information and an ITC hit

[2]Specifically, $|M(\psi^{(\prime)}) - M(\mu^+\mu^-)| > 100$ MeV/c^2 and $M(\psi^{(\prime)}) - M(e^+e^-) > 150$ MeV/c^2 or $M(e^+e^-) - M(\psi^{(\prime)}) > 100$ MeV/c^2 are required.

to create the B_s^0 candidates. The $D_s^- \ell^+$ vertex probability should be greater than 0.01% and the uncertainty on the B_s^0 decay length must be less than 0.5 mm. The requirements on the tracks used to form the vertices and on the vertex probabilities are somewhat different from the previous analysis[2]. Based on studies of the Monte Carlo simulation, these selection criteria give a 210 μm resolution on the B_s^0 decay length for the hadronic D_s^- decays. This resolution is similar to reference [2] with a slight reduction in the tails of the distributions. The B_s^0 decay length resolution is approximately 20% worse for the semileptonic D_s^- decay modes.

The reconstructed B_s^0 momentum for the $D_s^- \to \phi\pi^+\pi^-\pi^-$ mode must be at least 50% of the beam energy in order to reduce the greater combinatorial background. The $D_s^- \ell^+$ invariant mass should be in the range 3.0 to 5.5 GeV/c^2 (for $D_s^- \to \phi\ell^-\nu$ the lower bound is 2.5 GeV/c^2 because of the additional neutrino). This cut considerably reduces the $\overline{B} \to D_s^{(*)-} D^{(*)} X$ and $B \to D_s^- X_s \ell^+ \nu$ backgrounds[3].

The requirement that $L_{D_s^-}/\sigma(L_{D_s^-}) > -0.5$, where $L_{D_s^-}$ is the distance between the reconstructed B_s^0 and D_s^- vertices projected along the D_s^- direction, reduces the combinatorial background by approximately 50% and retains about 90% of the B_s^0 signal while inducing a very small bias on the B_s^0 decay length measurement. From a study of simulated B_s^0 semileptonic decays, this bias was determined to be -19 ± 3 μm. The bias was taken to be -20 μm with a 100% systematic uncertainty. For the average reconstructed B_s^0 momentum of 33 GeV/c, this leads to a bias of -0.01 ± 0.01 ps on the B_s^0 lifetime.

5 Sample composition

To determine the relative contributions of the signal and background processes in each channel, the D_s^- (ϕ) mass spectra are fitted with a Gaussian (Breit-Wigner) to represent the signal and a second degree polynomial to represent the combinatorial background for the hadronic (semileptonic) D_s^- decay modes. The masses are fixed to their nominal values[13] and the widths are fixed to their expected values determined from simulated semileptonic B_s^0 decays (Table 2). For the $D_s^- \to K^{*0}K^-$ channel, the fraction of the reflection background from $D^- \to K^{*0}\pi^-$ decays is fitted using a shape determined from the simulation. An additional Gaussian at the nominal D^- mass represents the contribution of the Cabibbo–suppressed hadronic decays of the D^-. The fitted mass spectra for the hadronic and semileptonic D_s^- decay modes are shown in Figure 1. The estimated contribution of the three main components within the mass windows (Table 2) is shown in Table 3 for each mode. A small correction has been applied to the $\phi e^- \nu$ yield to account for an estimated background of 0.9 ± 0.2 events due to hadrons misidentified as electrons. The small contribution of the $B \to D_s^- X_s \ell^+ \nu$ decay is considered as a systematic uncertainty only. The contribution to the $D_s^- \ell^+$ yield from $B_s^0 \to D_s^- \tau^+ \nu X$ followed by $\tau^+ \to \ell^+ \nu \overline{\nu}$ is estimated to be less than one event.

The reconstruction efficiencies for the signal and the mass resolution for each D_s^- decay mode are listed in Table 2. The reconstruction efficiency for the $\overline{B} \to D_s^{(*)-} D^{(*)} X$ background relative to the $B_s^0 \to D_s^- \ell^+ \nu$ signal for the hadronic and semileptonic D_s^- decays is determined to be 15.4 ± 1.4 % and 8.4 ± 1.2 %, respectively, where the uncertainties are due to the Monte Carlo statistics. For the $B \to D_s^- X_s \ell^+ \nu$ background, the relative efficiencies for the hadronic and semileptonic D_s^- decays are 54.2 ± 1.8 % and 39.0 ± 3.6 %, respectively.

Approximately 134 of the 208 $D_s^- \ell^+$ combinations are attributed to $B_s^0 \to D_s^- \ell^+ \nu X$ decays.

D_s^- decay mode	Mass resolution (MeV/c^2)	Mass cut (MeV/c^2)	$D_s^- \ell^+ \nu X$ efficiency(%)
$\phi\pi^-$	7.0	$\pm$ 15	9.7 ± 0.1
$K^{*0}K^-$	7.0	$\pm$ 15	6.2 ± 0.1
$K_s^0K^-$	10.0	$\pm$ 20	2.3 ± 0.1
$\phi\pi^+\pi^-\pi^-$	5.0	$\pm$ 10	5.7 ± 0.1
$K^{*0}K^{*-}$	7.0	$\pm$ 15	3.4 ± 0.1
$\phi e^-\nu$	4.7	$\pm$ 6	7.6 ± 0.2
$\phi\mu^-\nu$	4.7	$\pm$ 6	5.5 ± 0.2

Table 2: The second and third columns contain the D_s^- or ϕ mass resolution and mass acceptance window about the nominal D_s^- or ϕ mass for each mode. The signal detection efficiency is shown in the last column where the uncertainty is due to Monte Carlo statistics.

D_s^- decay mode	$D_s^- \ell^+ \nu X$ signal	$D_s^{(*)-}D^{(*)}X$ background	Combinatorial background	Total per mode
$\phi\pi^-$	36.7	3.6	6.7	47
$K^{*0}K^-$	47.0	4.3	23.6	76
$K_s^0K^-$	9.3	0.8	5.9	16
$\phi\pi^+\pi^-\pi^-$	9.8	0.9	9.3	20
$K^{*0}K^{*-}$	9.8	0.9	4.3	15
$\phi e^-\nu$	16.6	0.9	7.5	25
$\phi\mu^-\nu$	4.9	0.2	3.9	9
TOTAL	134.2	11.6	61.3	208

Table 3: The estimated contributions to the yield for each decay mode. The estimated contribution of one $D^- \to K^{*0}\pi^-$ event to the $K^{*0}K^-$mode is not shown in the table but is included in the totals.

6 Proper time reconstruction

The measured proper time of the B_s^0 is given by

$$t_m = \frac{M_{B_s^0} L_{B_s^0}}{p_{B_s^0}}$$

where $M_{B_s^0} = 5375 \pm 6$ MeV/c^2[13] is the mass of the B_s^0 , $L_{B_s^0}$ is the distance between the primary vertex and the $D_s^-\ell^+$ vertex projected on the $D_s^-\ell^+$ direction and $p_{B_s^0}$ is the B_s^0 momentum computed from the reconstructed D_s^- and lepton momenta and the neutrino energy estimated using the missing energy technique of reference [2]. Monte Carlo simulation shows that the B_s^0 boost resolution for the majority of the events is 5% as described in reference [2].

The temporal resolution is parametrized by a sum of two Gaussians and analytically convolved with the decay time distribution. The explicit expression for the probability density function for the

B_s^0 signal is

$$\tilde{P}(t_m;\tau_s) = \sum_{i=1}^{2} \rho_i \int_0^\infty dt \frac{1}{\sqrt{2\pi} S\sigma_i} e^{-\frac{1}{2}(\frac{t_m - t + \delta_i}{S\sigma_i})^2} \frac{1}{\tau_s} e^{-\frac{t}{\tau_s}}$$

where τ_s is the B_s^0 lifetime, ρ_i is the fractional contribution of the $i^{\rm th}$ Gaussian, δ_i is the offset and σ_i is the proper time resolution measured with the simulation. A scale factor S corrects for the differences in proper time resolution between the data and the simulation.

A separate parametrization of the proper time resolution for both the $B_s^0 \to D_s^- \ell^+ \nu$ and $B_s^0 \to D_s^{*-} \ell^+ \nu$ decays for each of the seven D_s^- decay modes is determined from Monte Carlo simulation with an input B_s^0 lifetime of 1.50 ps.

To determine S the negative part of the $L_{B_s^0}/p_{B_s^0}$ distribution is fitted with two Gaussians for "fake" $D_s\ell$ combinations in events where the *uds* content is enhanced to 50% by requiring the tracks in the hemisphere opposite to the B_s^0 candidate to be consistent with zero lifetime[11]. "Fake" $D_s\ell$ are candidates from either the like–sign $D_s\ell$ combinations, the unlike–sign $D_s\ell$ sideband or a D_s formed from the ϕ or K^* sidebands as defined in section 7. The ratio of the data to the simulation for the proper time resolution is measured to be $S = 1.2 \pm 0.1$.

Extensive analysis of simulated data with generated B_s^0 lifetimes of 1.0, 1.5 and 2.0 ps has shown that the parametrization of the temporal resolution as a sum of Gaussians yields an average bias of $-1.0 \pm 0.5\%$ on the fitted lifetime. This bias arises from neglecting the dependence of the proper time resolution on the proper time itself in the formulation of $\tilde{P}(t_m;\tau_s)$.

7 Lifetime fit

The likelihood function to be maximized for the lifetime fit is

$$\mathcal{L}(\tau_s) = \prod_{i=1}^{N} f_1 \tilde{P}(t_m^i;\tau_s) + f_2 \tilde{P}(t_m^i;\tau_d) + f_3 \tilde{P}(t_m^i;\tau_b) + f_4 B(t_m^i) \quad , \tag{1}$$

where

- f_1 is the relative fraction of $B_s^0 \to D_s^- \ell^+ \nu X$ events in the D_s^- or ϕ peak,
- f_2 is the relative fraction of $\overline{B} \to D_s^{(*)-} D^{(*)} X$ events,
- τ_d is the effective lifetime of the simulated $\overline{B} \to D_s^{(*)-} D^{(*)} X$ events,
- f_3 is the relative fraction of reflection background for $D_s^- \to K^{*0} K^-$,
- τ_b is the average b lifetime,
- f_4 is the relative fraction of combinatorial background,
- $B(t_m)$ is the proper time distribution of the combinatorial background, and
- N is the number of $D_s^- \ell^+$ candidates.

$B(t_m)$ is estimated from the proper time distributions of the candidates in the D_s^- and ϕ mass "sideband". For $D_s^\pm, \ell^\mp (\phi \ell^\pm \ell^\mp)$ candidates, the sideband extends from 2.05 to 2.30(1.021 to 1.120) GeV/c^2. For the like–sign candidates, $D_s^\pm, \ell^\pm (\phi \ell^\pm \ell^\pm)$, the lower limit of the sideband is reduced to 1.95(0.997) GeV/c^2. The proper time distributions for the hadronic and semileptonic D_s^- decays are separately parametrized by the sum of two Gaussians and two exponentials (one for $t_m < 0$ and one for $t_m > 0$).

Although not explicitly noted in eqn.(1), the f_i are calculated separately for each D_s^- decay mode as described in section 5.

The measured lifetime from the unbinned maximum likelihood fit for the entire data sample is $\tau(\mathrm{B_s}) = 1.56\ ^{+0.17}_{-0.15}$ ps (statistical uncertainty only) without correcting for the small biases due the parametrization of the resolution and the cut on $\mathrm{L_{D_s^-}}/\sigma(\mathrm{L_{D_s^-}})$. The proper time distribution and fit are shown in Figure 2.

7.1 Systematic uncertainties and corrections

The individual contributions to the systematic uncertainty on the $\mathrm{B_s^0}$ lifetime are summarized in Table 4 and discussed below.

Source	Uncertainty (ps)	
Combinatorial background	$+0.013$	-0.016
$\overline{\mathrm{B}} \to \mathrm{D_s^{(*)-}D^{(*)}}X$ background	$+0.023$	-0.016
$\mathrm{B} \to \mathrm{D_s^-}X_s\ell^+\nu$ background	$+0.001$	-0.009
Proper time resolution parametrization bias	$+0.008$	-0.008
Parametrization of proper time resolution	$+0.015$	-0.015
$\mathrm{L_{D_s^-}}/\sigma(\mathrm{L_{D_s^-}}) > -0.5$ bias	$+0.010$	-0.010
$\mathrm{B_s^0}$ boost resolution	$+0.010$	-0.010
Other	$+0.006$	-0.005
Total in quadrature	$+0.035$	-0.033

Table 4: The components of the estimated systematic uncertainty on the measured $\mathrm{B_s^0}$ lifetime. Additional details are described in the text.

The systematic uncertainty due to the combinatorial background is estimated by varying the calculated signal fraction of all decay modes by one standard deviation and by varying the proper time distribution of the combinatorial background, $B(t_\mathrm{m})$. The systematic uncertainty due to $B(t_\mathrm{m})$ is estimated by altering the parametrization (using a single Gaussian and two exponentials or by forcing the two Gaussians to have identical means), by using the unlike–sign or the like–sign sideband only, or by halving the width of the sidebands. In addition, a simultaneous fit to the signal and sidebands was performed similarly to the previous ALEPH measurement[2]. In this fit, the proper time distributions of the hadronic and semileptonic $\mathrm{D_s^-}$ sidebands were fitted separately with two non–zero lifetime components and a zero lifetime component.

The uncertainty due to the $\overline{\mathrm{B}} \to \mathrm{D_s^{(*)-}D^{(*)}}X$ background is estimated by varying both the calculated yield and the τ_d lifetime within their estimated uncertainties. For simulated $\overline{\mathrm{B}} \to \mathrm{D_s^{(*)-}D^{(*)}}X$ events, τ_d is fitted as 1.90 ± 0.20 ps, which is longer than the input b hadron lifetime of 1.50 ps due to the under–estimation of the boost. To account for the unknown multiplicity of "X" in the $\overline{\mathrm{B}}$ decay, the uncertainty has been increased to ± 0.30 ps. The uncertainty due to the $\mathrm{B} \to \mathrm{D_s^-}X_s\ell^+\nu$ decays is estimated by assuming that the rate is equal to the upper limit quoted earlier and varying the effective lifetime. The effective lifetime fitted for simulated $\mathrm{B} \to \mathrm{D_s^-}X_s\ell^+\nu$ is 1.75 ± 0.20 ps which also is longer than the input b hadron lifetime due to the under-estimated boost.

The lifetime is corrected by $+0.016 \pm 0.008$ ps for the bias observed in simulated $\mathrm{B_s^0} \to \mathrm{D_s^-}\ell^+\nu X$ events when they are fitted with the parametrization of the proper time resolution. An additional uncertainty arises due to the statistical precision in the parametrization of the proper time resolution and is estimated by varying the parameters by one standard deviation of their fitted values.

The lifetime is also corrected for the bias due to $\mathrm{L_{D_s^-}}/\sigma(\mathrm{L_{D_s^-}}) > -0.5$ by $+0.010 \pm 0.010$ ps which was described in section 4.3.

As in the previous measurement[2], the relative fractions of the tails of the reconstructed B_s^0 boost were varied by $\pm$ 20% to estimate the uncertainty due to the neutrino energy resolution. This yields an uncertainty of ± 0.010 ps. The B_s^0 momentum distribution was modified in the simulation and resulted in a negligible uncertainty in the lifetime.

The uncertainties due to following additional small effects are added in quadrature and are labeled as "Other" in Table 4:

- Monte Carlo studies show that if the lifetime to be measured differs substantially from the lifetime, $\tau_{\rm gen}$, used to create the parametrization of the proper time resolution (section 6), then the measured lifetime will be slightly biased towards $\tau_{\rm gen}$. This bias is treated as an additional systematic uncertainty by fitting the lifetime with parameters derived from different $\tau_{\rm gen}$ of 1.0, 1.5 and 2.0 ps.
- The scale factor for the proper time resolution is varied: $S = 1.2 \pm 0.1$.
- The estimated relative production rate of $B_s^0 \to D_s^{*-}\ell^+\nu$ to $B_s^0 \to D_s^-\ell^+\nu$ is approximated by the measured $B \to D^{(*)}\ell\nu$ rates[13] to be 2.3 ± 0.6.
- The mass of the B_s^0 meson is varied by 6 MeV/c^2[13].
- τ_b is varied by 0.05 ps.

The final result of the maximum likelihood fit for the B_s^0 lifetime, including the measurement biases, is

$$\tau(B_s^0) = 1.59\ ^{+0.17}_{-0.15}\ (\text{stat})\ \pm 0.03\ (\text{syst})\ \text{ps}\ .$$

8 Product branching ratio measurement

From yields of $D_s^-\ell^+$ combinations, it is possible to calculate the product branching ratio $\text{Br}(\bar{b} \to B_s^0) \cdot \text{Br}(B_s^0 \to D_s^-\ell^+\nu X)$, which can be used to estimate the production rate of B_s^0 mesons in $Z \to b\bar{b}$ decay.

Due to the sensitivity of such a measurement to the reconstruction efficiency, estimated from simulation, all requirements not essential to a yield measurement were removed: the requirements on the vertex probability, VDET and ITC assignments, the B_s^0 and D_s^- decay length resolution and the cut $L_{D_s^-}/\sigma(L_{D_s^-}) > -0.5$. The number of events within the mass acceptance windows (Table 2) and background estimates for the 3.1 million hadronic Z decays analysed are detailed in Table 5. The reconstruction efficiency estimates for signal and background processes are listed in Table 6. A likelihood function is constructed, taking into account the expected backgrounds in each channel. All channels are then simultaneously fitted for the product branching ratio.

The background processes are estimated as follows. The combinatorial background in each channel is estimated from the sidebands of the mass spectrum, fitted with a second-order polynomial, as described in section 5. The background due to real D_s^- mesons paired with misidentified hadrons or non-prompt leptons ("Accidental Combinations" in Tables 5 and 8) is expected to be small. In the $\phi\pi^-$ mode, it is estimated from a fit to the wrong-sign mass spectrum, then scaled by the ratio of right-sign to wrong-sign sideband events. As the other channels carry significantly less weight in the fit, this background in the other channels is scaled from the $\phi\pi^-$ channel. This yields a conservative error common to all modes. The reflection background is fitted directly in the mass spectrum of the $K^{*0}K^-$ decay mode, as described in section 5.

The background due to $\overline{B} \to D_s^{(*)-}D^{(*)}X$, $(D^{(*)} \to \ell^+\nu X)$ is estimated from the product of the inclusive branching ratio, $\text{Br}(B \to D_s^-X)$, measured at the $\Upsilon(4S)$[15, 16], and the average rate for secondary leptons in b decays, $\text{Br}(b \to c \to \ell)$, measured at LEP[21]. Combining these rates

Mode	Yield	Combin.	$D_s^{(*)-}D^{(*)}X$	Accid.	$D_s^- X_s \ell^+ \nu$	Signal
$\phi\pi^-$	145 ± 12.0	48.2 ± 1.6	15.3 ± 1.8	2.5 ± 8.1	8.2 ± 4.0	70.8 ± 15.2
$K^{*0}K^-$	257 ± 16.0	148.6 ± 2.9	12.0 ± 1.4	2.8 ± 9.0	6.4 ± 3.1	77.0 ± 19.6
$\phi e^- \nu$	102 ± 10.1	44.4 ± 1.8	4.6 ± 0.7	1.5 ± 4.8	3.4 ± 1.7	48.1 ± 11.5
$\phi\mu^-\nu$	53 ± 7.3	27.7 ± 1.5	3.0 ± 0.5	0.7 ± 2.1	2.4 ± 1.2	19.2 ± 7.8
$K_s^0K^-$	111 ± 10.5	83.8 ± 2.5	6.9 ± 0.8	0.7 ± 2.3	3.7 ± 1.8	15.9 ± 11.2
$\phi\pi^+\pi^-\pi^-$	180 ± 13.4	184.3 ± 2.7	5.7 ± 0.7	0.0 ± 0.4	3.1 ± 1.5	-13.0 ± 13.8
$K^{*0}K^{*-}$	55 ± 7.4	42.6 ± 1.8	2.7 ± 0.3	0.3 ± 1.0	1.5 ± 0.7	7.9 ± 7.7
Total	903 ± 30.0	579.6 ± 5.8	50.1 ± 2.6	8.5 ± 27.7	28.7 ± 14.0	225.9 ± 44.0

Table 5: Event yields and background estimates. The estimated contribution of 10.2 ± 5.1 reflection background events to the $K^{*0}K^-$ mode is not shown in the table but is included in the totals.

thus includes the contributions from the B_s^0 and from b baryons. The measured relative rate of two-body decays, $\Gamma(\overline{B} \to D_s^{(*)-}D^{(*)}) \,/\, \Gamma(B \to D_s^- X)$[15, 16], is used to calculate the efficiencies for this background (Table 7).

The background due to $B \to D_s^- X_s \ell^+ \nu$ is calculated as follows. The fraction of $B \to D_s^- X$ decays in which the D_s^- is not produced from the W^* ("lower vertex production") was recently measured to be $f_{\rm lower} = 0.172 \pm 0.083$, and a limit set at $f_{\rm lower} < 0.31$ at 90 % C.L.[17]. Combined with the inclusive D_s^- production rate, $\mathrm{Br}(B \to D_s^- X)$[15, 16], and the inclusive b semileptonic decay rate, $\mathrm{Br}(b \to X\ell\nu)$[21], the rate and limit for this background are estimated to be $\mathrm{Br}(B \to D_s^- X_s \ell^+ \nu) = 0.20 \pm 0.10$ % and < 0.36 % at 90 % C.L., respectively. These estimates are consistent with an earlier search[18] and theoretical estimates[19].

The calculated $B_s^0 \to D_s^- \ell^+ \nu X$ signal for each mode after subtraction of the estimated backgrounds is given in Table 5. Using the number of observed events, the estimated reconstruction efficiencies and background contributions, and the branching ratios in Table 7, the product branching ratio is simultaneously fitted to all seven decay modes. The result is

$$\mathrm{Br}(\overline{b} \to B_s^0) \cdot \mathrm{Br}(B_s^0 \to D_s^- \ell^+ \nu X) = 0.82 \ \pm 0.09 \ (\mathrm{stat}) \ {}^{+0.13}_{-0.14} \ (\mathrm{syst}) \ \%$$

which is the sum of the electron and muon decay channels divided by two[3]. The specific contributions to the systematic uncertainty are listed in Table 8.

9 Conclusion

The B_s^0 has been reconstructed in the semileptonic decay mode $B_s^0 \to D_s^- \ell^+ \nu X$ using seven different D_s^- decay modes in approximately 3 million hadronic Z decays. The result of an unbinned, maximum likelihood fit to the B_s^0 lifetime for the observed 208 $D_s^- \ell^+$ combinations is

$$\tau(B_s^0) = 1.59 \ {}^{+0.17}_{-0.15} \ (\mathrm{stat}) \ \pm 0.03 \ (\mathrm{syst}) \ \ \mathrm{ps}$$

[3]The product branching ratio quoted in reference [7] was calculated neglecting $B \to D_s^- X_s \ell^+ \nu$; including this process, $f(b \to B_s^0)$ is $11.0 \pm 1.2 \, {}^{+2.5}_{-2.6}$ % and $f(b \to B_d^0)$ is $38.8 \pm 1.3 \pm 2.1$ %. The baryon fraction remains unchanged, $f(b \to \Lambda_b) = 11.5 \pm 2.2 \pm 3.4$ %.

Mode	$B_s^0 \to D_s^- \ell^+ \nu X$	$\overline{B} \to D_s^{(*)-} D^{(*)} X$	$B \to D_s^- X_s \ell^+ \nu$
$\phi\pi^-$	$16.5 \pm 0.1\,\%$	$3.7 \pm 0.3\,\%$	$9.7 \pm 0.2\,\%$
$K^{*0}K^-$	$10.1 \pm 0.2\,\%$	$2.3 \pm 0.2\,\%$	$5.9 \pm 0.2\,\%$
$\phi e^- \nu$	$17.9 \pm 0.3\,\%$	$2.1 \pm 0.2\,\%$	$7.5 \pm 0.5\,\%$
$\phi\mu^-\nu$	$13.4 \pm 0.3\,\%$	$1.4 \pm 0.2\,\%$	$5.3 \pm 0.5\,\%$
$K_s^0 K^-$	$10.6 \pm 0.2\,\%$	$2.4 \pm 0.2\,\%$	$6.2 \pm 0.2\,\%$
$\phi\pi^+\pi^-\pi^-$	$12.1 \pm 0.2\,\%$	$2.7 \pm 0.2\,\%$	$7.1 \pm 0.2\,\%$
$K^{*0}K^{*-}$	$5.9 \pm 0.1\,\%$	$1.3 \pm 0.1\,\%$	$3.5 \pm 0.1\,\%$

Table 6: Reconstruction efficiencies for signal and physics background processes. The uncertainties are due to Monte Carlo statistics.

Quantity	Value	Source
R_b	0.2204 ± 0.0020	[20]
$Br(D_s^- \to \phi\pi^-)$	$3.5 \pm 0.4\ \%$	[13]
$\Gamma(D_s^- \to K^{*0}K^-) / \Gamma(D_s^- \to \phi\pi^-)$	0.95 ± 0.10	[13]
$\Gamma(D_s^- \to \phi\ell^-\nu) / \Gamma(D_s^- \to \phi\pi^-)$	0.54 ± 0.05	[13]
$\Gamma(D_s^- \to K_s^0 K^-) / \Gamma(D_s^- \to \phi\pi^-)$	1.01 ± 0.16	[13]
$\Gamma(D_s^- \to \phi\pi^+\pi^-\pi^-) / \Gamma(D_s^- \to \phi\pi^-)$	0.51 ± 0.12	[13]
$\Gamma(D_s^- \to K^{*0}K^{*-}) / \Gamma(D_s^- \to \phi\pi^-)$	1.6 ± 0.6	[13]
$Br(\phi \to K^+K^-)$	$49.1 \pm 0.9\ \%$	[13]
$Br(K_s^0 \to \pi^+\pi^-)$	$68.61 \pm 0.28\ \%$	[13]
$Br(B \to D_s^- X)$	$10.46 \pm 0.73\ \%$	[15, 16]
$\Gamma(\overline{B} \to D_s^{(*)-} D^{(*)}) / \Gamma(B \to D_s^- X)$	$52.8 \pm 6.1\ \%$	[15, 16]
$Br(b \to \ell\nu X)$	$11.08 \pm 0.31\ \%$	[21]
$Br(b \to c \to \ell)$	$8.22 \pm 0.46\ \%$	[21]
$\Gamma(B \to D_s^- X)_{\text{lower vertex}} / \Gamma(B \to D_s^- X)$	0.172 ± 0.083	[17]

Table 7: Rates used in the calculation of the product $Br(\overline{b} \to B_s^0) \cdot Br(B_s^0 \to D_s^- \ell^+ \nu X)$ and in estimating background process contributions. Additional details are given in the text.

Source	Uncertainty (%)	
$\mathrm{Br}(\mathrm{D_s^-} \to \phi\pi^-)$	$+0.106$	-0.085
Accidental combination background	$+0.030$	-0.097
$\mathrm{B} \to \mathrm{D_s^-} X_s \ell^+ \nu$ background	$+0.045$	-0.045
Other branching ratios	$+0.036$	-0.039
$\overline{\mathrm{B}} \to \mathrm{D_s^{(*)-}} \mathrm{D}^{(*)} X$ background	$+0.016$	-0.016
Combinatorial background	$+0.016$	-0.015
Reflection background	$+0.013$	-0.012
$\mathrm{R_b}$	$+0.008$	-0.007
Efficiency estimates (simulation)	$+0.005$	-0.005
Total	$+0.128$	-0.144

Table 8: Sources of systematic uncertainty in percent on the product branching ratio $\mathrm{Br}(\overline{b} \to \mathrm{B_s^0}) \cdot \mathrm{Br}(\mathrm{B_s^0} \to \mathrm{D_s^-} \ell^+ \nu X)$.

in agreement with the results from reference [12]. An alternative and independent ALEPH measurement using $\mathrm{D_s^-}$ -hadron correlations[24] found $\tau(\mathrm{B_s^0}) = 1.61\ ^{+0.30}_{-0.29}$ (stat) $^{+0.18}_{-0.16}$ (syst) ps using data from 1991 to 1993. The two ALEPH results can be combined to give

$$\tau(\mathrm{B_s^0}) = 1.59\ ^{+0.15}_{-0.14}\ \mathrm{ps}\ ,$$

which is consistent with the $\mathrm{B_d^0}$ lifetime 1.58 ± 0.06 ps[25], as expected from theoretical considerations[1].

The product branching ratio is measured to be

$$\mathrm{Br}(\overline{b} \to \mathrm{B_s^0}) \cdot \mathrm{Br}(\mathrm{B_s^0} \to \mathrm{D_s^-} \ell^+ \nu X) = 0.82\ \pm 0.09\ (\mathrm{stat})\ ^{+0.13}_{-0.14}\ (\mathrm{syst})\ \%\ ,$$

in agreement with previous measurements[3, 22, 23].

Acknowledgements

It is a pleasure to thank our colleagues in the accelerator divisions of CERN for the excellent performance of the LEP accelerator. Thanks are also due to the technical personnel of the collaborating institutions for their support in constructing and maintaining the ALEPH experiment. Those of us not from member states wish to thank CERN for its hospitality.

References

[1] I.I. Bigi *et al.*, in *B Decays*, Revised 2nd Edition, edited by S. Stone (World Scientific, Singapore, 1994).

[2] D. Buskulic *et al.*, ALEPH Collaboration, Phys. Lett. **B322** (1994) 275.

[3] D. Buskulic *et al.*, ALEPH Collaboration, Phys. Lett. **B294** (1992) 145, which assumed $\mathrm{Br}(\mathrm{D_s^-} \to \phi\pi^-) = 2.7 \pm 0.7\%$.

[4] D. Buskulic *et al.*, ALEPH Collaboration, "Limit on $\mathrm{B_s^0}$ oscillation using a jet charge method," CERN-PPE/95-084 (June 1995), to be published in Phys. Lett. **B**.

[5] D. Buskulic *et al.*, ALEPH Collaboration, Phys. Lett. **B322** (1994) 441.

[6] R. Akers *et al.*, OPAL Collaboration, Z. Phys. **C66** (1995) 555.

[7] D. Buskulic *et al.*, ALEPH Collaboration, "A Measurement of $|\mathrm{V_{cb}}|$ from $\overline{\mathrm{B}}^0 \to \mathrm{D}^{*+}\ell^-\overline{\nu}_\ell$", CERN-PPE/95-094 (July 1995), submitted to Phys. Lett. **B** .

[8] D. Decamp *et al.*, ALEPH Collaboration, Nucl. Instrum. Methods **A294** (1990) 121.
G. Batignani *et al.*, 1991 IEEE Nuclear Science Symposium, Santa Fe, IEEE Trans. Nucl. Sci. NS-39(4/5) (1992) Vol. 1, p. 438.

[9] D. Buskulic *et al.*, ALEPH Collaboration, Nucl. Instrum. Methods **A360** (1995) 481.

[10] D. Decamp *et al.*, ALEPH Collaboration, Z. Phys. **C53** (1992) 1.

[11] D. Buskulic *et al.*, ALEPH Collaboration, Phys. Lett. **B313** (1993) 535.

[12] P.D. Acton *et al.*, OPAL Collaboration, Phys. Lett. **B312** (1993) 501;
P. Abreu *et al.*, DELPHI Collaboration, Z. Phys. **C61** (1994) 501;
F. Abe *et al.*, CDF Collaboration, Phys. Rev. Lett. **74** (1995) 4988;
R. Akers *et al.*, OPAL Collaboration, Phys. Lett. **B350**, (1995) 273.

[13] L. Montanet *et al.*, Particle Data Group, Phys. Rev. **D50** (1994) 1173.

[14] D. Buskulic *et al.*, ALEPH Collaboration, Nucl. Instrum. Methods **A346** (1994) 461.

[15] T. Bergfeld *et al.*, CLEO Collaboration, "Measurements of $B \to D_s^+ X$ Decays," Contribution to the 27th International Conference on High Energy Physics, Glasgow, Scotland, 20-27 July, 1994, ICHEP94 Ref. GLS-0246 and CLEO preprint CLEO CONF 94-9.

[16] H. Albrecht *et al.*, ARGUS Collaboration, Z. Phys. **C54** (1992) 1.

[17] X. Fu *et al.*, CLEO Collaboration, "D_s - Lepton Charge Correlations in B Meson Decays: A Study of the D_s Meson Production Mechanism," Contribution to the International Europhysics Conference on High Energy Physics, Brussels, Belgium, 27 July - 2 August, 1995, Ref. EPS-0169 and CLEO preprint CLEO CONF 95-11.

[18] H. Albrecht *et al.*, ARGUS Collaboration, Z. Phys. **C60** (1993) 11.

[19] E. Golowich *et al.*, Z. Phys. **C48** (1990) 89.

[20] U. Uwer, "LEP Results on Electro-Weak Physics from Quarks," Proceedings of the 30th Rencontres de Moriond (Les Arcs, Savoie, France) March 1995.

[21] ALEPH, DELPHI, L3, OPAL and The LEP Electroweak Working Group, "Combined Preliminary Data on Z Parameters from the LEP Experiments and Constraints on the Standard Model," CERN-PPE/94-187.

[22] P. Abreu *et al.*, DELPHI Collaboration, Phys. Lett. **B289** (1992) 199.

[23] P.D. Acton *et al.*, OPAL Collaboration, Phys. Lett. **B295** (1992) 357.

[24] D. Buskulic *et al.*, ALEPH Collaboration, "Measurement of D_s^+ meson production in Z decays and of the $\overline{B}_s^0$ lifetime," CERN-PPE/95-092, (June 1995) submitted to Z. Phys. **C**.

[25] V. Sharma, "Recent measurements of b hadron lifetimes," Proceedings of the 6th International Symposium on Heavy Flavour Physics, (Pisa, Italy) June 1995.

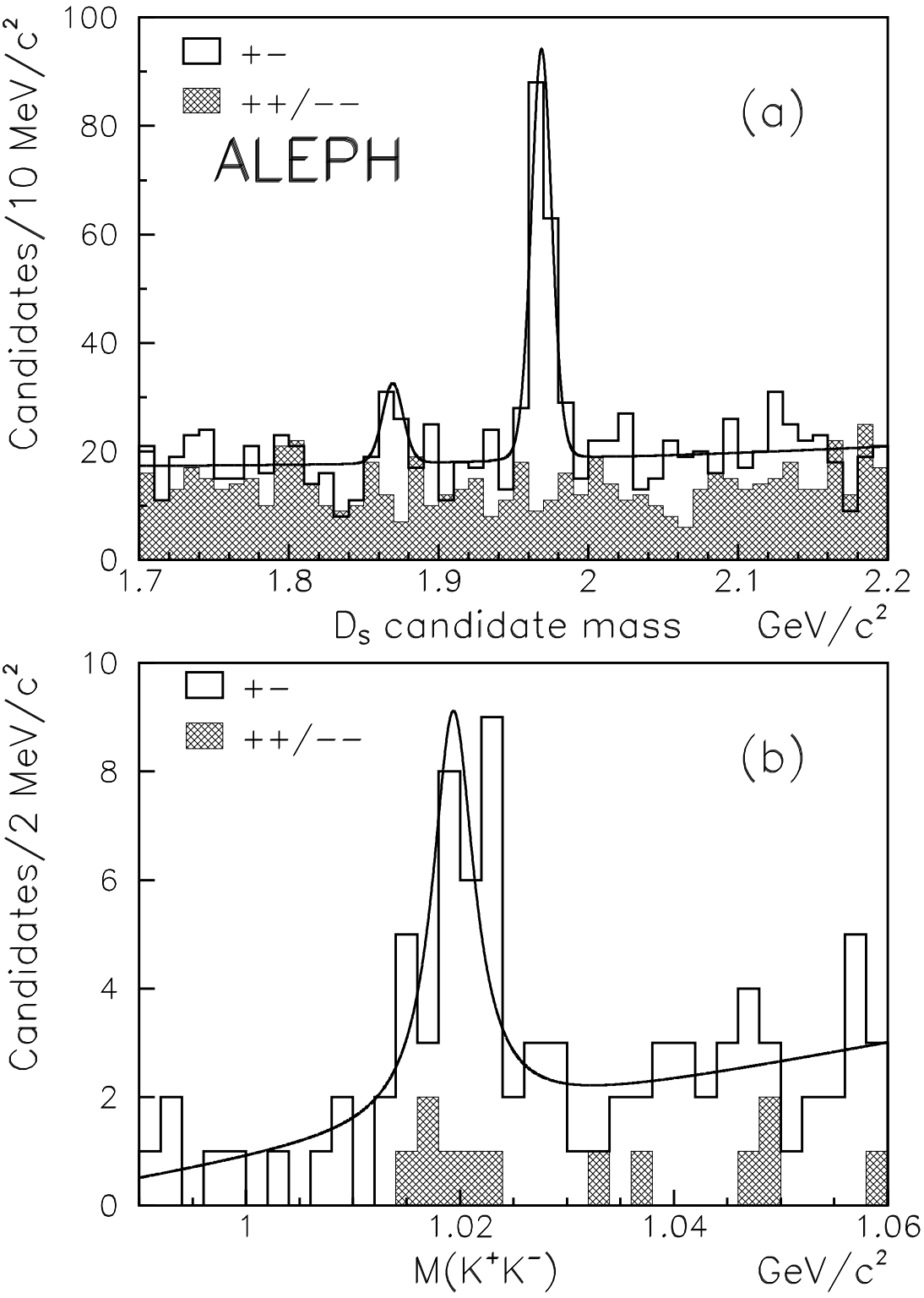

Figure 1: (a) The mass distribution of the D_s^- candidates for $D_s^-\ell^+$ combinations for hadronic D_s^- decays, and (b) the K^+K^- mass distribution for semileptonic D_s^- decays, showing the fits described in the text. The shaded histograms represent the like–sign mass spectra.

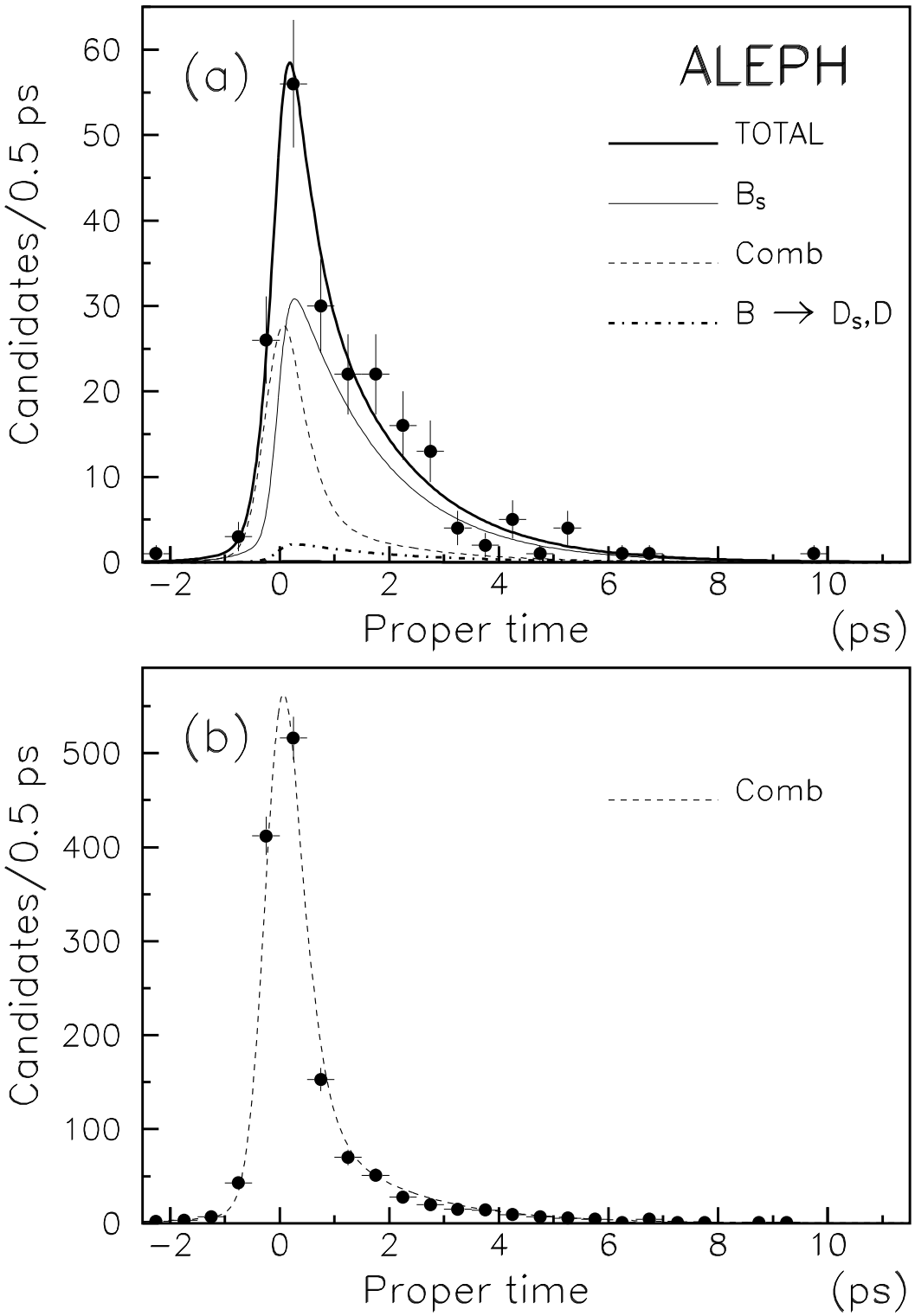

Figure 2: The proper time distributions of (a) the $D_s^- \ell^+$ events in the D_s^- and ϕ mass window showing the fitted contributions of the signal and the combinatorial and $\overline{B} \rightarrow D_s^{(*)-} D^{(*)} X$ backgrounds as described in the text. (b) The fit to the proper time distribution of the events in the $D_s^- \ell^+$ sideband and the like–sign events.